Deformation of Heated and Loaded Wooden Stick
Towards Fire Safety Design of Timber Structure

Wang, Supan; Zhang, Ziyang; Nan, Zhuojun; Liu, Yanhui; Huang, Xinyan

DOI
10.1016/j.cscm.2025.e04452

Publication date
2025

Document Version
Final published version

Published in
Case Studies in Construction Materials

Citation (APA)
Wang, S., Zhang, Z., Nan, Z., Liu, Y., & Huang, X. (2025). Deformation of Heated and Loaded Wooden Stick: Towards Fire Safety Design of Timber Structure. *Case Studies in Construction Materials*, *22*, Article e04452. https://doi.org/10.1016/j.cscm.2025.e04452

Case Studies in Construction Materials 22 (2025) e04452

Contents lists available at ScienceDirect

Case Studies in Construction Materials

journal homepage: www.elsevier.com/locate/cscm

Case study

Deformation of heated and loaded wooden stick: Towards fire safety design of timber structure

Supan Wang [a,b], Ziyang Zhang [a], Zhuojun Nan [c], Yanhui Liu [b,*], Xinyan Huang [b,*]

[a] College of Safety Science and Engineering, Nanjing Tech University, Nanjing, China
[b] Research Centre for Smart Urban Resilience and Firefighting, Department of Building Environment and Energy Engineering, The Hong Kong Polytechnic University, Hong Kong
[c] Faculty of Architecture, Delft University of Technology, Delft, Netherlands

ARTICLE INFO

Keywords:
Timber fire safety
Wood dehydration
Fire resilience
Three-point test
Finite element analysis

ABSTRACT

Mass timber construction has been emerging in architecture because of exceptional durability, sustainability, and versatility. This work applies the 3-point bending test to a reduced-scale wooden stick with a supporting span of 16.5 cm, under loads up to 560 times its self-weight under raised environmental temperatures up to 300 °C in the oven. The experiments quantify the deformation, critical shear stress of rupture, and degradation mass losses of the heated wood before ignition and combustion, while the numerical model further analyses the detailed thermomechanical responses. Results show that with increasing temperature, the deflection of loaded wooden sticks increases, driven by drying, thermal creep deformation, and thermal degradation. Moreover, the critical shear stress and temperature for wooden sticks rupture decrease, primarily caused by the thermal degradation of wood. The effects of fire-scene temperature on bending strength and modulus of elasticity on the loss of load-bearing capacity for wooden sticks are further quantified with numerical simulation. This work reveals the pre-ignition thermo-mechanical behaviours of wood under fire scenes, which supports early warnings for ignition and collapse, fire resilience design, and structural-fire stability assessment for wooden structures.

1. Introduction

Wood has been extensively employed for millennia as a significant structural element for building construction due to exceptional durability, sustainability, and versatility [1–3]. For example, most ancient architecture in China was wooden, which was perceived as the distinctive symbol of Chinese architectural culture [4,5]. More than 80 % of residential buildings in North America have been made of wood since 2015, and some will serve more than 100 years [1]. Timber structures have gained popularity again in recent years because of exceptional durability, sustainability, and versatility [6–10]. High-rise and landmark mass timber constructions are emerging, such as the 'HAUT' timber-hybrid building in Amsterdam and Mjøstårnet—The Wood Hotel in Norway.

However, all wood materials are vulnerable to combustion under fire because they are the most common fuel that can feed the flame and increase fire hazards [11–13]. Although timber elements provide a certain degree of fire resistance through the formation of charring layers, the protective charring layers can fail under severe burning conditions, leading to the structural failure of wooden buildings [14–16]. In 2014, a fire quickly spread and engulfed a village within 1.5 h in southwest China (Fig. 1a), destroying the

* Corresponding authors.
E-mail addresses: yanhui2021.liu@connect.polyu.hk (Y. Liu), xy.huang@polyu.edu.hk (X. Huang).

https://doi.org/10.1016/j.cscm.2025.e04452
Received 13 November 2024; Received in revised form 22 January 2025; Accepted 24 February 2025
Available online 27 February 2025

200-year-old wooden-structure buildings [17]. In April 2019, a catastrophic fire broke out in the Notre Dame Paris Cathedral [18]. The wooden roof deformed and collapsed under fire, which caused a huge loss for human civilisation (Fig. 1b). In 2014, a modern wooden-framed laboratory at the University of Nottingham caught fire [19], requiring the efforts of 60 firefighters to finally bring the blaze under control (Fig. 1c). Thus, the conservation of historical timber buildings and the development of modern timber-framed structures are restricted by fire safety issues.

When exposed to fire, the timber element undergoes thermal expansion, thermal degradation, and combustion, accompanied by different levels of deformation, which may eventually lead to the collapse of the timber structure. To improve the fire performance of wooden structures, considerable research efforts have been devoted to combustion, which includes pyrolysis, ignition, and burning. Roberts [20] systematically reviewed the kinetics data for the wood pyrolysis. As the major components of wood, the hemicellulose, cellulose, and lignin could be pyrolysed at 200–260 °C, 240–350 °C, and 280–500 °C, respectively. During pyrolysis, each component transfers into active species and decomposes into char and gas products [21]. Particularly, charring is of great significance for the fire resistance design of timber structures [2,16]. The char on the wood surface can act as an insulating layer to prevent the underlying timber from fire, slowing the thermal penetration [22].

Nevertheless, the charring process reduces the effective cross-section since the char is of zero strength. Understanding the wood charring is also essential for assessing the residual load-bearing capacity of timber structures under fire [23]. Therefore, key influencing factors on charring characteristics such as chemical composition [24,25], timber precessing [26], wood ageing [27], external heating [28–31], oxygen permeability [32,33], joints locations [34], and loading conditions [16,35] have been studied by many researchers. Assuming that the pyrolysis processes of the three main components of wood are independent, Richter *et al.* [24,25] numerically investigated the effect of chemical composition and oxygen concentration on the charring process. Results indicated that the kinetics had negligible influence on charring prediction across scales, while the physical properties deserved more attention in modelling. Qin *et al.* [35] found that adding mechanical loads could deteriorate the stability of wood by increasing the charring rate and charring depth under fire exposure. Recently, Gangi *et al.* [16] conducted a numerical investigation into the impact of plywood stacking sequences on its mechanical behaviours in the fire exposure tests, accurately predicting the mechanical response of wood samples at different scales. Apart from wood combustion, developing external fireproof coating materials is also an emerging research topic, and nano-scale fire retardants are being researched and extended [36,37].

Although studies have focused on the characteristics of the combustion process and the development of fire retardants, limited research has investigated the thermomechanical behaviour of timber elements under mechanical loading at elevated temperatures, especially from the perspective of fire safety design [16]. Wang *et al.* [38] observed the four successive deformation stages during the wood dehydration, pyrolysis, oxidation and verified heterogeneous processes, and thermomechanical stresses for each deformation stage by numerical simulation. Wiesner *et al.* [39] investigated the effect of adhesive on structure failure for cross-laminated timber (CLT) walls under external thermal radiation and found interactions between adhesive choice and ply thickness on the structural capacity of CLT. Lineham *et al.* [40] studied the structural response of CLT beams exposed to fire under sustained flexural loading, highlighting the limitations of the current study and recommending more detailed thermo-mechanical analyses towards realistic structural fire safety design. Therefore, understanding timber deformation in the early stage of heating exposure is still needed, especially for the effects of load and thermal conditions. To improve the fire resilience of timber structures and ensure safe egress [41], studying the deformation of loaded timber beams under fire exposure and figuring out the underlying mechanisms is crucial.

Toward the fire-safe design of timber structures, this work first conducted experiments on small-scale loaded wood beams in an oven to investigate their deformation under high temperatures. The deflection and mass loss of wooden sticks were measured, and the critical temperature to trigger the wooden stick break was determined. Afterwards, numerical simulations were performed to reproduce the experiments and reveal a more detailed thermomechanical analysis, providing a scientific guideline for the early warning of fire hazards, reliable fire safety design, and structural fire stability evaluation of wooden structures.

2. Experimental methods

2.1. Wood sample and test procedure

Cross-laminated timbers are increasingly popular in construction. This study examined the thermomechanical responses of loaded

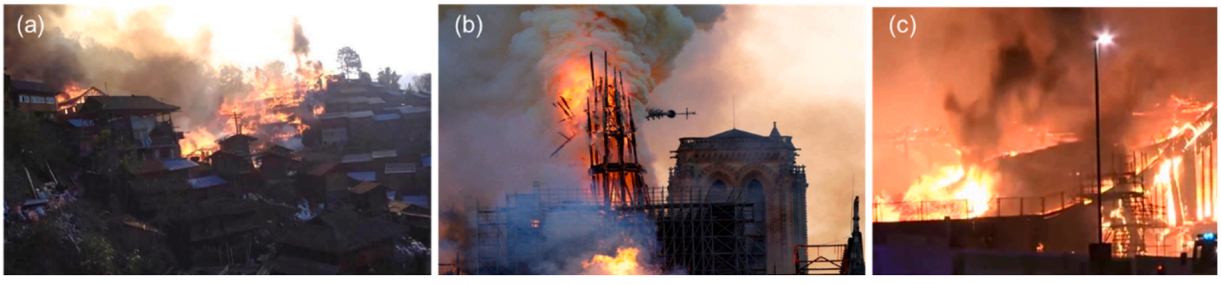

Fig. 1. Photographs of (a) the 2014 fire in Jianhe historical town, Guizhou, China [17], (b) the Notre-Dame de Paris fire in 2019 [18], and (c) the fire occurred in the wooden framed laboratory at the University of Nottingham.

CLT lamellas, designed as wooden sticks, using a series of small-scale three-point tests at elevated temperatures in an oven. The wood-stick sample used in this work was the typical beech wood cut perpendicular to the grains, i.e., a widely used material in furniture manufacturing and building construction. It had a density of 800 ± 70 kg/m^3 and moisture content of 12 ± 1 % at the ambient temperature of 27 °C and relative humidity of 60 %. The dimensions of the wooden sticks were identical for all tests, namely, 200 mm × 20 mm × 5 mm for length × width × thickness (Fig. 2a). The weight of the wooden stick sample was 16 ± 1 g, so it was much lower than the applied load (up to 9 kg). The maximum ratio of load to sample self-weight was about 560, so the self-weight of wooden sick could be ignored.

The schematic diagram of the experimental setup is illustrated in Fig. 2b. The 3-point bending test setup was placed inside the hot oven to control the environmental temperature and simulate the heating in different fire scenes. The hot oven can provide a constant gas-phase temperature of up to 330 °C with a thermal stability of ±1 °C at 1 atm. The test sample was put on the fixture inside the oven with a load (up to 9 kg) applied to the mid-span of the wooden stick, and the supporting span was around 16.5 cm. For a standard three-point bending test, the maximum shear stress in a rectangular cross-sectional timber beam under a point load in the centre can be expressed as [42],

$$\tau_{\max} = \frac{3F_b}{4bh} \tag{1}$$

where F_b is the load at a given point; b and h are the width and the depth of the wooden stick, respectively. In this study, the maximum shear stress for the loads with 1 kg, 3 kg, 5 kg, 7 kg, and 9 kg are calculated in Table 1.

Considering that it is difficult to monitor the mass loss of the testing wooden sticks with load, we set a twin sample without the load inside the oven as a reference to record its mass loss fraction. Note that this work focuses on the deformation mechanism of loaded timber beams at elevated temperatures before the ignition and combustion processes. The mass loss of the sample was recorded by the electric balance (resolution: 0.01 g). Before the test, the oven was preheated to the desired temperature and then stabilised for at least 10 min. Afterwards, the sample with the expected load was placed on a stainless-steel supporting frame in the oven, as shown in Fig. 2c. It took about 2–3 min to open the oven and set the sample loading in the oven. After the oven was reclosed, it took another 2–3 min for the oven to return to the pre-set temperature, which was set as the time zero of the deformation.

This work aims to find the critical ambient temperature for the wood break. Experiments were conducted under different oven temperatures from 150 °C to 250 °C and at the step of 25 °C. We defined the lowest oven gas-phase temperature to trigger the break of loaded wooden sticks as supercritical temperature. In contrast, the subcritical temperature is the highest gas-phase temperature, preventing the loaded wooden sticks from breaking. The tests were ended until the temperature difference between the supercritical and subcritical temperatures was within 50 °C. Then, the critical ambient temperature triggers the wooden sticks to break (T_a^*) could be regarded as the average value of supercritical and subcritical temperatures.

To ensure experimental repeatability, the test under the same conditions (both the given load and gas-phase temperature) was repeated at least four times. During the tests, a digital camera was used to monitor the deformations, and the deflections were acquired by image processing accordingly.

2.2. Deformation phenomena

Fig. 3 presents the deformation process of the wooden sticks with a maximum shear stress of 368 kPa at 150 °C, where the white dotted rectangle represents the initial position of the non-loaded wooden stick. The deflection w (mm) was measured, and the MATLAB-based image processing program was employed to calculate and calibrate the accurate deflection value of experimental cases. Initially, the stick deformed slightly due to the load and short heating effect. After around 0.5 h, the deformation became more significant, indicating the reduction of structural stability. Nevertheless, the increase in deflection was not visible to the naked eye directly after 1 h. Therefore, Fig. 3 does not show the experimental phenomena after 3 h.

Fig. 4a demonstrates the deformation and mass evolution of the wooden stick with a maximum shear stress of 368 kPa at 150 °C

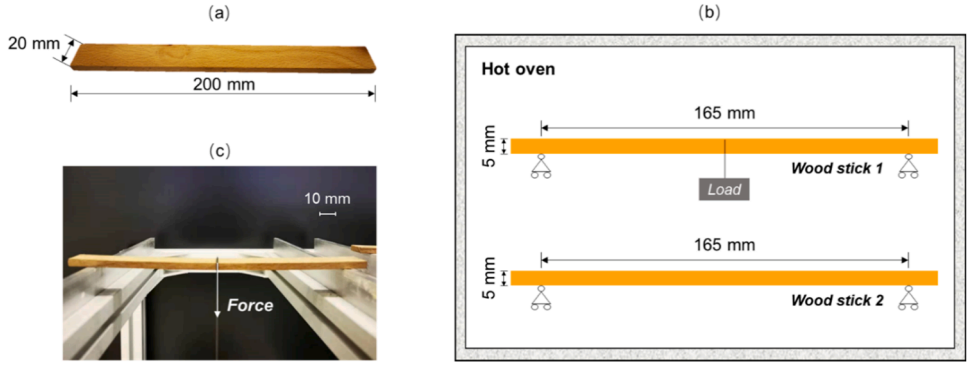

Fig. 2. (a) Photo of the wooden stick sample, (b) schematic diagram of the experimental setup, and (c) photo of the 3-point test setup.

Table 1
The maximum shear stress under the given loads.

Load (kg)	1	3	5	7	9
Maximum shear stress (kPa)	74	221	368	515	662

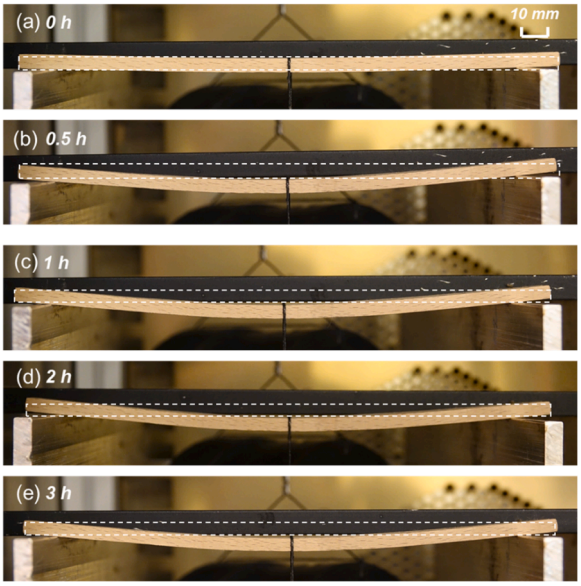

Fig. 3. The deformation process of the wooden stick with a maximum shear stress of 74 kPa at 150 °C.

(the case in Fig. 3). When exposed to heating, the deflection rapidly increased to 4.41 mm in the first 0.5 h and reached a constant of 5.28 mm after one hour. Initially, the wooden stick deflected by 0.66 mm due to the mechanical load. At 0.5 h, the mass fraction decreased to a constant of 88 %, indicating that the mass loss of this case was attributed to the water evaporation. After that, the mass fraction did not change, implying the wood would not be pyrolysed at this temperature (i.e., 150 °C). Therefore, the deflection rate decreased with the heating duration from 0.5 h to 1 h, which is attributed to the decrease in the elastic modulus as the wood changes from wet to dry for a given extent. After the experiment, the colour of the wooden stick deepened (Fig. 4a) due to the generation of a small number of phenolic compounds and aromatic compounds [43]. Wood colour is closely related to the modulus of rupture (MOR) and modulus of elasticity (MOE), which could be used to evaluate the mechanical strength of wood [44].

Elevating the oven temperature to 200 °C, the deflection and mass evolution curves of the wooden stick are plotted in Fig. 4b. At the beginning, the deflection was 2.48 mm, which was larger than the initial value in Fig. 4a because of the higher gas-phase temperature. Similarly, the deflection rapidly raised to 10.5 mm during the first 0.5 h, implying the reduction of structural stability compared with

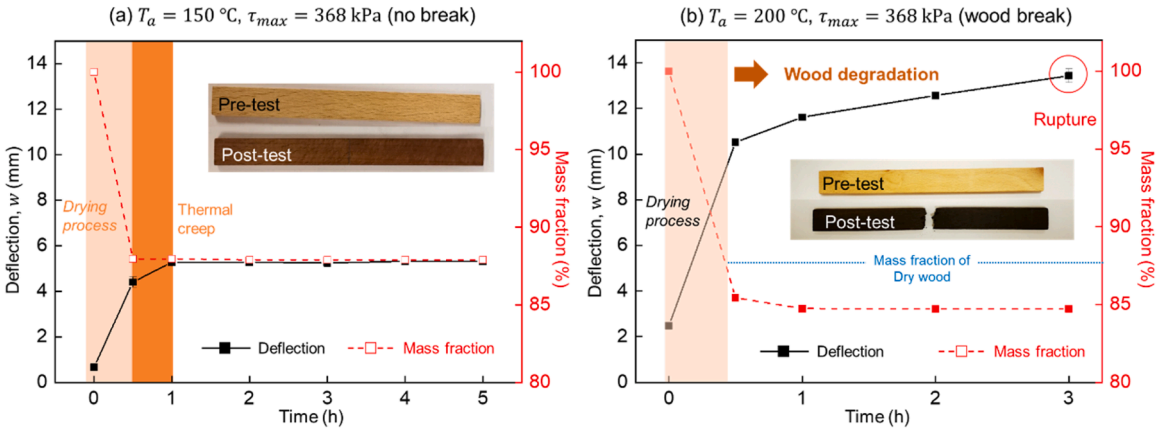

Fig. 4. Deflection and mass evolution curves of wood beams with the 368-kPa shear stress at the ambient temperature of (a) 150 °C (no break), and (b) 200 °C (break).

the environment of 150 °C. According to the mass fraction curve in Fig. 4b, the drying process was completed in less than 0.5 h. The mass loss of the wooden stick did not stop after the water evaporation, indicating the occurrence of strong thermal degradation. Although the deflection rate slowed down after 0.5 h, the deflection continuously increased until it broke at 3 h. Before its rupture, the maximum deflection was measured as 13.43 mm. As illustrated in Fig. 4b, the mass fraction decreased from 100 % to 85 % within 3 h, and the colour of the entire wooden stick changed to black after the experiment.

2.3. Critical temperature to trigger the wooden stick rupture

The shear stress levels varying with the temperature to trigger the wooden stick break are summarised in Fig. 5a. This figure illustrates the relationship between temperature and corresponding shear stress that impacts the load-bearing capacity of the timber beam, highlighting the conditions under which failure is most likely to occur. As expected, the shear stress for timber failure decreases as temperature increases. Specifically, the shear stress decreases from 662 kPa to 74 kPa as gas-phase temperature increases from 150 °C to 250 °C. Thus, it can be concluded that both temperature and shear stress exacerbate wooden stick deformation. Normally, increasing the temperature will reduce the strength of construction materials. However, increasing the applied load (and thereby increasing the shear stress) does not inherently reduce the strength of construction materials. Increasing the load does not reduce the inherent strength; it simply brings it closer to its failure point. The fitted correlation in Fig. 5a can aid in estimating the failure of the loaded wooden stick under various temperatures.

To investigate the failure mechanism of the timber beam, the relationship between critical temperature and mass fraction at wooden stick rupture is plotted in Fig. 5b. Since the moisture content of this sample is 12 ± 1 %, the dry-based mass fraction is marked in this figure. Interestingly, the mass loss of the wooden stick with a 662 kPa stress at the rupture moment was lower than 11 %, indicating that it was broken before the drying process was completed. Therefore, in this case, the mechanical load predominantly drove the wood rupture.

For the wooden sticks with shear stress lower than 662 kPa, their mass fractions at the rupture moment were larger than their dry-based mass fraction. For example, the critical temperature for the wooden stick at 74 kPa stress is around 225 °C, which is higher than the pyrolysis temperature of the wood as determined by thermogravimetric (TG) measurements [45]. The 38 % mass loss implies the occurrence of strong pyrolysis. The mass loss is larger than 12 % when the temperature is higher than 175 °C, suggesting the onset of pyrolysis in this temperature range. Note that this temperature (i.e., 175 °C) is lower than the pyrolysis temperature, as is the difference between the continuous heating condition in the small-scale oven used in this work and the transient thermal environments in TG tests. In conclusion, the failure of wooden sticks was mainly ascribed to thermal degradation. The current work aims to study the deformation behaviour before the combustion process. Therefore, relatively large loads were applied to induce significant deformation, and the oven temperatures were controlled to avoid the combustion of the wooden sticks.

2.4. Analytical solution for wood deformation

Considering the case of the loaded wood beams at the subcritical condition, the deflection will eventually reach a constant (Fig. 4a). For simplicity, we regard the length of the wooden sticks as the beam span since the minor distance between the wood edge and the bearing could be negligible. As illustrated in Fig. 6, the sample is placed on two supporting pins (AC), has a constant flexural rigidity (EI), and a given force (F_b) acts on the mid-span (B). w_B represents the maximum deflection at the mid-span B.

In the current experimental setup, the deflection at the central location w_B $(x = \frac{l}{2})$ is [46]

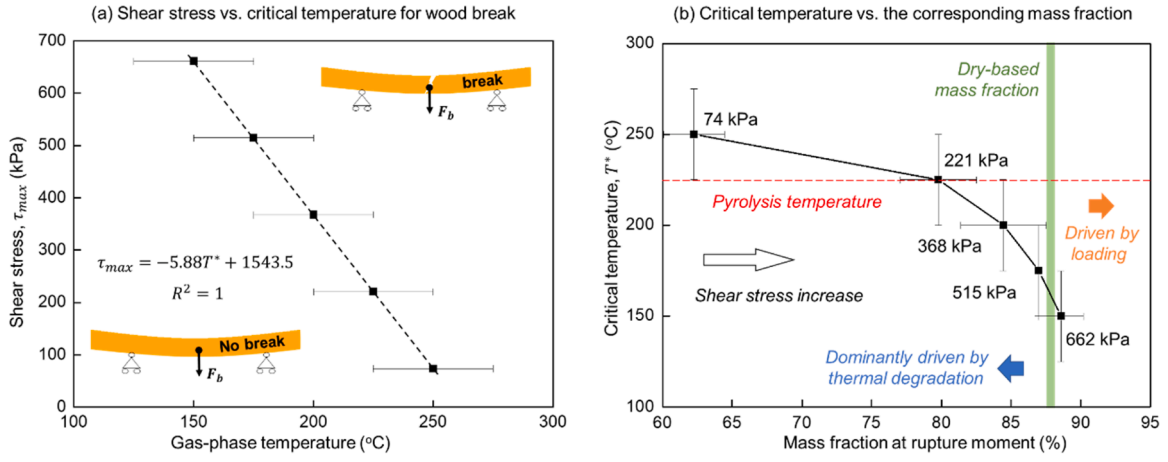

Fig. 5. (a) The shear stress varying with the gas-phase temperature to trigger the wooden stick break, and (b) the corresponding mass fraction at rupture moment.

$$w_B = \frac{1}{48EI} F_b l^3 = \frac{F_b}{EI}\left(1.67 \times 10^{-4}\right) \quad [m] \tag{2}$$

Thus, the flexural rigidity of the wood beam can be expressed as

$$EI = \frac{F_b l^3}{48 w_B} = \frac{F_b}{w_B}\left(1.67 \times 10^{-4}\right) \quad [N \bullet m^2] \tag{3}$$

Based on the measured maximum deflection at mid-span, the corresponding flexural rigidity could be regarded as the effective maximum bending stiffness EI_e under the high temperature. As shown in Fig. 7, this bending stiffness decreases with increasing temperatures. It should be noted that all values in Fig. 7 are accompanied by error bars, but the error bars for the last two values are too small to be clearly visible. The underlying mechanism needs further numerical study.

3. Numerical simulation

3.1. Model setup

To further investigate the deformation of timber beams under heating and to understand the effects of temperature and moisture content on mechanical properties and stress-strain behaviour, a simplified 2D numerical model is established using the commercial software COMSOL. The numerical model is developed based on the experimental setup. The sample has dimensions of 200 mm (length) × 20 mm (width) × 5 mm (thickness). The mechanical and fire loads applied to the timber beams in various simulation cases are also based on the experimental setup. The gas-phase temperature in the oven is applied as the thermal boundary on the timber beams for subsequent heat transfer analysis. Significant mass loss due to thermal degradation only occurred for the oven temperature of 250 °C. The gas-phase temperature used in the simulations are lower than pyrolysis temperature (e.g., 225 °C), and therefore thermal degradation is not considered, and the heterogeneous chemistry can be simplified by drying as

$$\text{wet wood} \rightarrow \nu_{d,dr}\text{dry wood} + \nu_{g,dr}H_2O \tag{4}$$

The condensed-phase conservation equations of mass, species, and energy are presented as

$$\frac{\partial \overline{\rho}}{\partial t} = -\overline{\rho}_0(1-\nu_{d,dr})\dot{\omega}'''_{\mathrm{dr}} \tag{5}$$

$$\frac{\partial y_w}{\partial t} = -\dot{\omega}'''_{\mathrm{dr}}, \quad \frac{\partial y_d}{\partial t} = \nu_{d,dr}\dot{\omega}'''_{dr} \tag{6}$$

$$(\overline{\rho c})\frac{\partial T}{\partial t} = \nabla(\overline{k}\nabla T) + \sum_k \overline{\rho}_0 \dot{\omega}'''_{\mathrm{dr}} \Delta H_{\mathrm{dr}} \tag{7}$$

where $\overline{\rho}$, $\overline{c}$, and $\overline{k}$, are the average density, specific heat, and thermal conductivity of the wooden sticks, respectively. ΔH_{dr} and $\dot{\omega}'''_{\mathrm{dr}}$ are heat of reaction and reaction rate of dehydration or drying. The kinetic model and chemical kinetic parameters of drying are based on [38].

In this model, the timber beams are restrained in vertical displacement only, making the beam simply supported at both ends, and a point load F_p is applied at the mid-span. For 2D components, the thermo-elasticity formulation is based on the equilibrium equations.

$$\nabla\vec{\sigma} + \vec{F_v} = 0 \tag{8}$$

where $\nabla\vec{\sigma}$ is the stress tensor of the material and $\vec{F_v}$ represents the overall body load, including the external load and gravity. The expression for the stress tensor can be written according to the general Hook's law as

$$\vec{\sigma} = C : (\vec{\varepsilon} - \vec{\varepsilon_{th}}) \tag{9}$$

where $\overline{C}$ is the symmetric elasticity tensor (containing Young's modulus E and Poisson's ratio μ), and $\vec{\varepsilon_{th}}$ is the thermal strain tensor, respectively. The initial Young's modulus E is shown in Table 2. The total strain tensor $\vec{\varepsilon}$ is written by the displacement $\vec{u}$ as

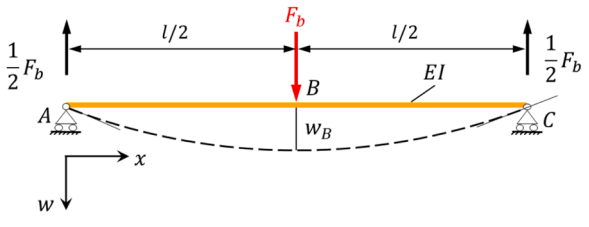

Fig. 6. Schematic for analysing the wooden stick sample used in the three-point bending test.

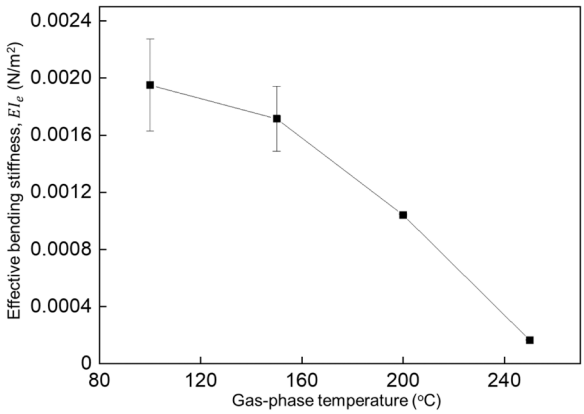

Fig. 7. The effective maximum bending stiffness EI_e plotted for the corresponding temperature.

$$\overrightarrow{\varepsilon} = \frac{1}{2}\left[(\nabla \overrightarrow{u})^T + \nabla \overrightarrow{u} + (\nabla \overrightarrow{u})^T \nabla \overrightarrow{u}\right] \tag{10}$$

The above strain tensor can also be rewritten as

$$\overrightarrow{\varepsilon} = \overrightarrow{\varepsilon_{th}} + \overrightarrow{\varepsilon_e} + \overrightarrow{\varepsilon_p} = \alpha \Delta T + \overrightarrow{\varepsilon_e} + \overrightarrow{\varepsilon_p} \tag{11}$$

where $\overrightarrow{\varepsilon_e}$ is elastic strains, $\overrightarrow{\varepsilon_p}$ is plastic strains, α and ΔT are the thermal expansion tensor and the temperature change, respectively. In this model, y_i is the volumetric fraction of species i, X_i is the mass fraction of species i, and i contains wet wood and dry wood. The averaged properties in each cell are calculated as

$$\overline{\rho} = \sum X_i \rho_i, \quad \overline{c} = \sum X_i c_i, \quad \overline{k} = \sum Y_i k_i, \quad \overline{C} = \sum Y_i \overline{C}_i, \quad X_i = \overline{\rho}\frac{Y_i}{\rho_i} \tag{12}$$

The wood properties are summarised in Table 2, and based on the experimental samples.

Eqs. (4–12) are solved with the transient-state solution by finite element methods, using the GMRES (Generalised Minimal Residual) iteration method. The domains are discretised into 202 triangular meshes, and an initial time step is 180 s (3 min). When the mesh size or time step decreases by a factor of 2, the numerical results vary less than 0.5 %, so the mesh or time resolution is well solved.

3.2. *Effect of the temperature on wood deformation and stress*

Fig. 8a shows the simulation results of deformation under a 368-kPa shear stress at the temperature of 150 °C from 0 s to 10800 s (3 h). In most of cases, the deformation of the timber beam occurred before 1800 s (0.5 h). Fig. 8b compares the deformations of the wooden stick obtained from the experiment and simulation under 50 N load at temperatures of 150 °C and 200 °C. The deformation of the wooden stick loaded with 368-kPa shear stress at 150 °C changed rapidly after 3000 s. For the wooden stick with the same load at 200 °C, the deflection rate decreased after 2500 s. However, the deformation increased over time until the plastic strain in some parts exceeded 60 %, eventually leading to fracture. It is clear that the mechanical properties of wood degrade and become more prone to deformation or fracture as the temperature increases. This result aligns with the experimental observations in the previous section, and the trend of deformation development is consistent.

Fig. 9 illustrates the development of (a) the wood stick temperature at the centre of the cross-section at the mid-span of the timber beam and (b)residual mass fraction at different gas-phase temperatures. The different heating conditions of 100 °C, 150 °C, 175 °C, 200 °C, 225 °C, and 250 °C were simulated. When the temperature exceeds 250°C, the thermal oxidation might become significant. To ensure the accuracy of the simulation results, the scenario with an ambient temperature of 250 °C is not considered in Fig. 9. The results show that the beam temperature under all heating conditions increases rapidly from 0 to 100 s and reaches a stable state (equal to the gas temperature) within 150 s. The model only considered thermal evaporation; therefore, the mass loss was all due to the evaporation of water. According to the experiment, the reactants and products were dry wood (800 kg/m^2) and wet wood (700 kg/m^2), respectively, i.e., the moisture content was 12.5 %. With increasing gas-phase temperatures, there is a significant change in the

Table 2
Physical parameters of wet and dry wood in the model [38].

Species	ρ (kg/m^3)	c (J/kg·K)	k (W/m·K)	E (Pa)	μ	α (1/K)
Wet wood	800	2128.6	0.384	0.9e8	0.384	2.7 * 10^{-4}
Dry wood	700	1900	0.324	1.17e8	0.384	2.7 * 10^{-4}

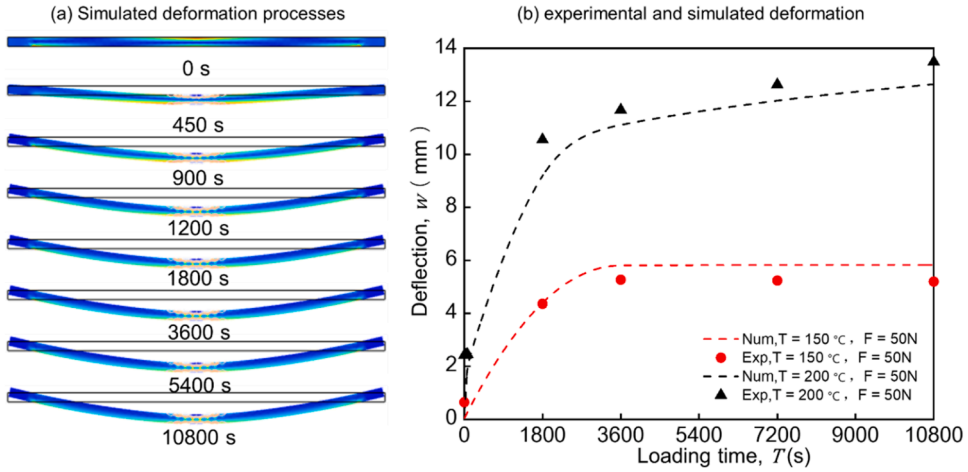

Fig. 8. Deformation development of the wooden stick under a 50 N load (same as the 368-kPa shear stress): (a) simulation results at a temperature of 150°C, and (b) comparison of the experimental and simulated deformations at temperatures of 150 °C and 200 °C.

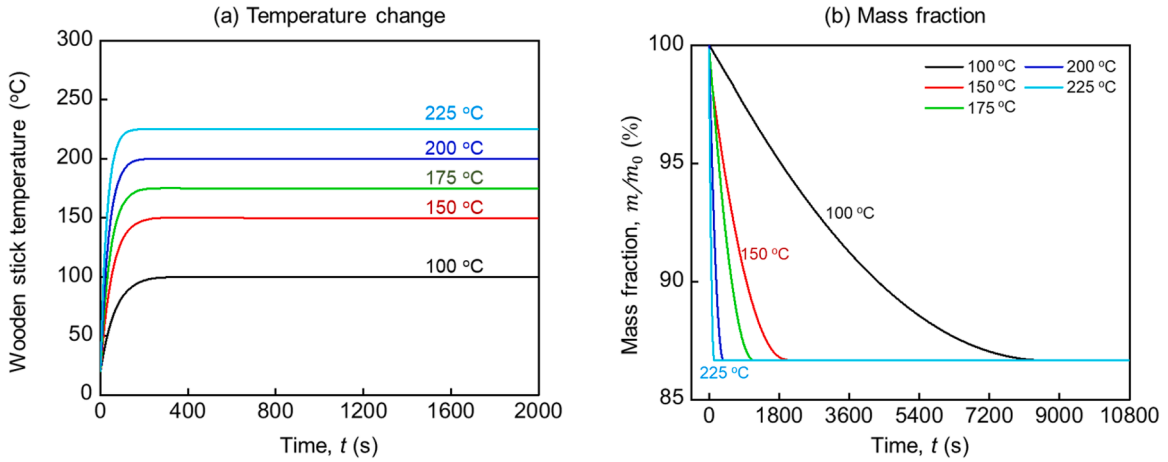

Fig. 9. The evolution curves of (a) beam temperature at the centre of the cross-section at the mid-span of the wooden stick (x = 100 mm, y = 5 mm) and (b) mass fraction at gas-phase temperatures ranging from 100 °C to 250 °C.

development of the residual mass fraction (see Fig. 9b). At the gas temperature of 100 °C, the rate of mass loss significantly slows down after 3600 s, and the timber beam is completely converted to dry wood by approximately 8500 s. When the gas temperature rises to 150 °C, it takes about 1900 s for evaporation, which is also consistent with the experimental results shown in Fig. 4b. For heating conditions from 175 °C to 225 °C, the moisture evaporates rapidly within 100 s – 900 s.

Based on the simulated results above, the heating condition of 200 °C with a 50 N point load is selected to further investigate the relative stress (σ/σ_{max}) in relation to the development of temperature and mass fraction, as shown in Fig. 10. After loading, the relative stress rapidly increases from 0 % to 23 %, rises to 45 % at 100 s, and then is followed by a short decline, marking the yield point of the wooden stick where plastic strain begins to develop. Subsequently, the relative stress increases again, reaching the peak value of 100 % at around 250 s. This phenomenon is similar to the necking of metallic materials, and the rate of plastic strain generation increased with the material gradually starting to fail since that point. Therefore, up to about 800 s, the internal stress decreased quickly once again due to plastic strain, corresponding to the large degree of deformation at that time in Fig. 8b. After 800 s, the rate of stress reduction decreased until fracture occurred. In addition, it can be observed from Fig. 9 that the rate of stress rise remained almost the same as that of temperature rise, and their highest points almost coincided. Relatively, the moisture content of the sample still declined fast when the stress reached the maximum. Therefore, we can suppose that temperature has a greater effect on wood mechanical properties than moisture content.

3.3. Effect of the heating condition on bending strength and modulus of elasticity

We further investigated the effect of heating conditions on the mechanical properties of wood. The evolution of relative bending

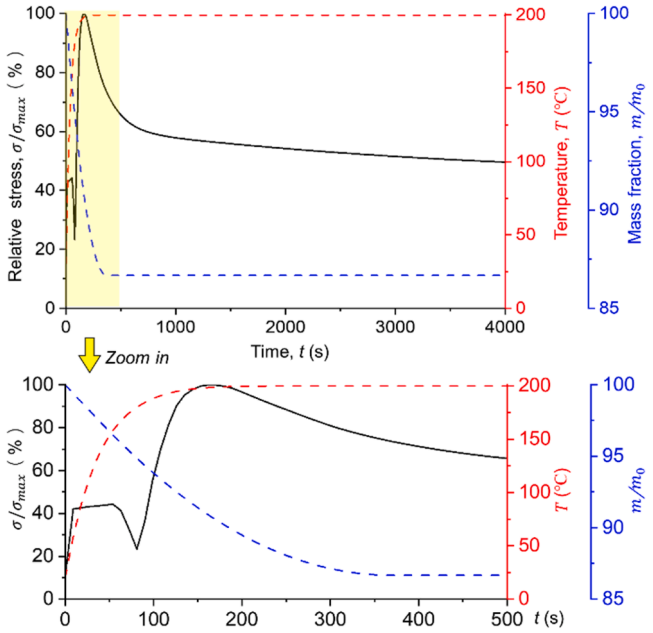

Fig. 10. Relative stress ($\sigma/\sigma_{\max}$) under 200 °C with the 368-kPa stress in relation to temperature and mass fraction development.

strength and relative modulus of elasticity with varying gas-phase temperatures are shown in Fig. 11. The bending strength R can be defined as

$$R = \frac{3F_b L}{2bh^2} \tag{13}$$

where F_b is the given point load, and L, b, h are the length, width and thickness of the timber beam, respectively. Once the deflection is larger than 10 mm, the deflection will increase until the timber beam fractures. F_b was calculated and taken from the various loads that caused fracture at different ambient temperatures. Due to the 2-D model, we considered h as 1. Taking the bending strength at 150 °C as the benchmark, it fell to 30 % when the ambient temperature rose to 200 °C. As the temperature continued to grow, the decline in bending strength slowed down, with about 10 % remaining at 250 °C. We can infer that the bending strength of wood rapidly weakens by 70 % at a temperature increase from 150 °C to 200 °C and that the flexural capacity declines substantially during this temperature interval.

The relative modulus of elasticity was calculated by equivalent numerical simulation with the same load at ambient temperature (20 °C). As the gas-phase temperature rose from 150 °C to 200 °C, only 10 % of the modulus of elasticity remained, and then the rate of reduction slowed down, closing to 0 % at 250 °C. This trend is consistent with the bending strength and effective maximum bending stiffness calculated in Section 2.4. The stiffness EI of the wood was also extremely weak at this point, and it can be assumed that the wood member had completely lost its load-bearing capacity.

Although the simplified 2D numerical model proposed in this study successfully describes the deformation of loading wooden beams in a hot atmosphere, it may only apply to the specific conditions and type of wooden stick (cross-grained wood) examined here. Future work will investigate the thermomechanical responses of wood with different grain patterns, and the scale-effect will be considered under varied thicknesses, lengths, and loading conditions. We also plan to develop a 3D model with improved generalization capabilities to simulate actual timber structures and fire scenarios better.

4. Conclusions

In this work, a series of 3-point bending tests were performed for a small horizontal bench wooden stick (cross-grained wood) under a supporting span of 16.5 cm, ambient temperature up 300 °C, and loads up to 560 times self-weight. The effects of ambient pressure on wood deformation extent, critical shear stress of rupture, and degradation mass losses are comprehensively investigated. Experimental results suggest that the deformation of loaded wood can occur before combustion, which intensifies with the rising ambient temperatures. The critical shear stress for wood rupture decreases from 662 kPa to 74 kPa as ambient temperature increases from 150 °C to 250 °C.

To reveal a more detailed thermomechanical process, a simplified 2-D numerical model is established to further describe the deformation of loading wood beams in a hot atmosphere. The model aptly reproduced the experimental deformation process, and the results match that of the experiment. The temperature, mass loss and stress evolution of the sample were obtained. Analysis shows that the temperature has a greater effect on wood mechanical properties compared to the moisture content, and the deterioration of the

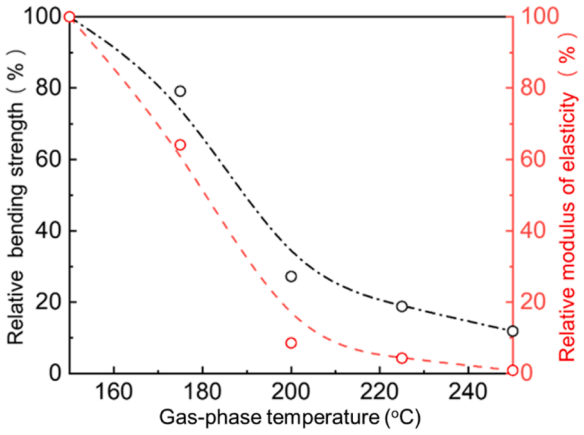

Fig. 11. Evolution of relative bending strength and relative modulus of elasticity with varying gas-phase temperatures.

mechanical properties of wood is mainly concentrated between 150 °C and 200 °C. By 250 °C, the member can be considered to fail. The relative ambient temperature on bending strength and modulus of elasticity have been calculated to characterise the loss of load-bearing capacity on wood members. This work can provide a scientific guideline for the early warning of thermal hazards, reliable fire safety design, and structural stability evaluation for wooden structures in different fire scenarios.

CRediT authorship contribution statement

Wang Supan: Writing – original draft. **Zhang Ziyang:** Writing – review & editing, Data curation. **Nan Zhuojun:** Writing – review & editing. **Liu Yanhui:** Writing – original draft, Investigation, Formal analysis, Data curation. **Huang Xinyan:** Writing – review & editing, Funding acquisition, Conceptualization.

Declaration of Competing Interest

The authors declare that they have no known competing financial interests or personal relationships that could have appeared to influence the work reported in this paper.

Acknowledgements

The work described in this paper was supported by grants from the National Natural Science Foundation of China (52176113, 52322610) and the University Natural Science Research Project in Jiangsu Province (21KJA620003).

Appendix

The wood samples were pulverised into powders, and then the thermogravimetric (TG) measurement was performed. The PerkinElmer STA 6000 Simultaneous Thermal Analyzer was employed, where two atmospheric gas flows were selected, i.e., nitrogen and air. The samples with 3-mg initial mass were heated at a constant rate of 10 K/min. Experiments were repeated twice and exhibited good repeatability. The decomposition temperature of the sample is around 200 °C (Fig. A1), lower than the critical rupture temperature of the sample with 74 kPa shear stress. Thus, the TG results can further validate that the rupture of wood with low shear stress is mainly driven by its thermal degradation.

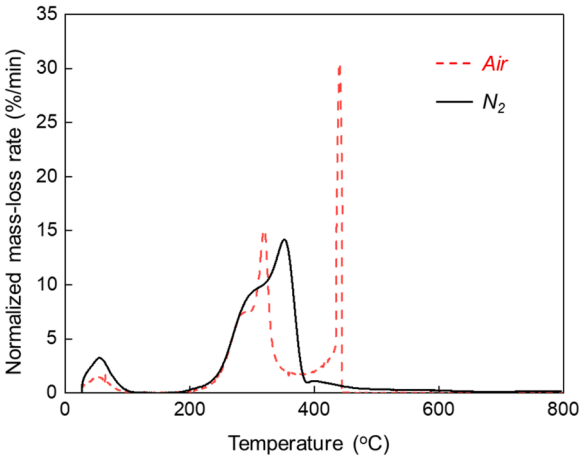

Fig. A1. TG results of the wood sample under air and nitrogen flow at a heating rate of 10 K/min

Data availability

Data will be made available on request.

References

[1] F. Asdrubali, B. Ferracuti, L. Lombardi, C. Guattari, L. Evangelisti, G. Grazieschi, A review of structural, thermo-physical, acoustical, and environmental properties of wooden materials for building applications, Build. Environ. 114 (2017) 307–332.
[2] C. Fan, Y. Gao, Y. Li, L. Yan, D. Zhu, S. Guo, et al., A flame-retardant densified wood as robust and fire-safe structural material, Wood Sci. Technol. 57 (2023) 111–134.
[3] D. Casagrande, D. Brandon, G. D'Arenzo, C. Viau, Design of taller timber buildings subjected to accidental loads: a state-of-the-art review, COST Action CA (2022) 20139.
[4] L.H. Chang, X.H. Chang, H. Chang, W. Qian, L.T. Cheng, The predictive research of ancient wooden building internal defects compressive bearing capacity based on nondestructive testing methods, Mech. Adv. Mater. Struct. 28 (2019) 252–259.
[5] J. Zhao, X. Jiang, J. Song, S. Lu, Y. Xiao, C.M. Shu, Influence of natural aging on wood combustion heat release, Wood Sci. Technol. 58 (2024) 1227–1257.
[6] D. Barber, Tall timber buildings: what's next in fire safety, Fire Technol. 51 (2015) 1279–1284.
[7] C. Chen, Y. Kuang, S. Zhu, I. Burgert, T. Keplinger, A. Gong, et al., Structure–property–function relationships of natural and engineered wood, Nat. Rev. Mater. 5 (2020) 642–666.
[8] J. Song, C. Chen, S. Zhu, M. Zhu, J. Dai, U. Ray, et al., Processing bulk natural wood into a high-performance structural material, Nature 554 (2018) 224–228.
[9] X. Estrella, P. Guindos, J.L. Almazán, S. Malek, Efficient nonlinear modeling of strong wood frame shear walls for mid-rise buildings, Eng. Struct. 215 (2020) 110670.
[10] S. Huč, T. Hozjan, R. Pečenko, Thickness of zero-strength layer in timber beam exposed to fuel-controlled parametric fires, Wood Sci. Technol. 57 (2023) 929–944.
[11] S.L. Zelinka, L.E. Hasburgh, K.J. Bourne, Wood & Fire Safety, Springer International Publishing, 2020.
[12] C. Gorska, J.P. Hidalgo, J.L. Torero, Fire dynamics in mass timber compartments, Fire Saf. J. 120 (2020) 103098.
[13] J. Liu, E.C. Fischer, Review of large-scale CLT compartment fire tests, Constr. Build. Mater. 318 (2022) 126099.
[14] S. Lin, Y. Qin, X. Huang, M. Gollner, Use of pre-charred surfaces to improve fire performance of wood, Fire Saf. J. 136 (2023) 103745.
[15] A.I. Bartlett, R.M. Hadden, L.A. Bisby, A review of factors affecting the burning behaviour of wood for application to tall timber construction, Fire Technol. 55 (2019) 1–49.
[16] M.J. Gangi, B.Y. Lattimer, S.W. Case, Scale modeling of thermo-structural fire tests of multi-orientation wood laminates, Wood Sci. Technol. 58 (2024) 1285–1322.
[17] Xinhua, Fire engulfs ethnic village in SW China. China Daily, 2014.
[18] K.E. Smith, D. Weis, C. Chauvel, S. Moulin, Honey maps the Pb fallout from the 2019 fire at Notre-Dame Cathedral, Paris: a geochemical perspective, Environ. Sci. Technol. Lett. 7 (2020) 753–759.
[19] University of Nottingham laboratory fire probed by safety officers. *BBC NEWS* 2014.
[20] A.F. Roberts, A review of kinetics data for the pyrolysis of wood and related substances, Combust. Flame 14 (1970) 261–272.
[21] I. Vermesi, M.J. DiDomizio, F. Richter, E.J. Weckman, G. Rein, Pyrolysis and spontaneous ignition of wood under transient irradiation: experiments and a-priori predictions, Fire Saf. J. 91 (2017) 218–225.
[22] F. Wiesner, F. Randmael, W. Wan, L. Bisby, R.M. Hadden, Structural response of cross-laminated timber compression elements exposed to fire, Fire Saf. J. 91 (2017) 56–67.
[23] V. Babrauskas, Charring rate of wood as a tool for fire investigations, Fire Saf. J. 40 (2005) 528–554.
[24] F. Richter, A. Atreya, P. Kotsovinos, G. Rein, The effect of chemical composition on the charring of wood across scales, Proc. Combust. Inst. 37 (2017) 4053–4061.
[25] F. Richter, F.X. Jervis, X. Huang, G. Rein, Effect of oxygen on the burning rate of wood, Combust. Flame 234 (2021) 111591.
[26] Y. Zhang, Z. Su, W. Ni, X. Zhang, L. Wang, Experimental study and theoretical analysis of fire resistance properties of prestressed glued laminated timber beams, Constr. Build. Mater. 424 (2024) 135967.
[27] B. Chorlton, J. Gales, Fire performance of cultural heritage and contemporary timbers, Eng. Struct. 201 (2019) 109739.
[28] M. Audebert, D. Dhima, A. Bouchaïr, Proposal for a new formula to predict the fire resistance of timber connections, Eng. Struct. 204 (2020) 110041.
[29] Hirashima T., Yamashita H., Ishi S., Igarashi T., Baba S., Someya T. Deformation behaviour and failure time of glued laminated timber columns in fire. The 11th International Conference on Structures in Fire, 2020.

[30] Li Y. Factors Affecting the Structural Integrity of Wood-Based Composites: Elevated Temperature and Adhesive Bonding, Virginia Tech, 2021.
[31] Z. Liang, S. Lin, X. Huang, Smoldering ignition and emission dynamics of wood under low irradiation, Fire Mater 47 (2023) 514–524.
[32] E. Hugi, M. Wuersch, W. Risi, K. Ghazi Wakili, Correlation between charring rate and oxygen permeability for 12 different wood species, J. Wood Sci. 53 (2007) 71–75.
[33] Y. Qin, Y. Zhang, Y. Chen, S. Lin, X. Huang, Minimum oxygen supply rate for smouldering propagation: effect of fuel bulk density and particle size, Combust. Flame 261 (2024) 113292.
[34] M. Sciomenta, J.L. Vihmann, E. Tuhkanen, A. Just, M. Fragiacomo, The effects of timber species and adhesive type on the behavior of finger joints in tension under fire conditions, Constr. Build. Mater. 448 (2024) 138080.
[35] R. Qin, A. Zhou, C. Lun, D. Lau, Structural performance and charring of loaded wood under fire, Eng. Struct. 228 (2020) 111491.
[36] L. Lowden, T. Hull, Flammability behaviour of wood and a review of the methods for its reduction, Fire Sci. Rev. 2 (2013) 1–19.
[37] W. Chu, J. Fang, Y. Yang, S. Tao, H.R. Shah, M. Wang, et al., Reaction to fire of the timber structure encapsulated by multilayer mortar coating under uniform thermal loading, Fire Technol. 61 (2024) 183–212.
[38] S. Wang, P. Ding, S. Lin, X. Huang, A. Usmani, Deformation of wood slice in fire: Interactions between heterogeneous chemistry and thermomechanical stress, Proc. Combust. Inst. 38 (2021) 5081–5090.
[39] F. Wiesner, R. Hadden, S. Deeny, L. Bisby, Structural fire engineering considerations for cross-laminated timber walls, Constr. Build. Mater. 323 (2022) 126605.
[40] S.A. Lineham, D. Thomson, A.I. Bartlett, L.A. Bisby, R.M. Hadden, Structural response of fire-exposed cross-laminated timber beams under sustained loads, Fire Saf. J. 85 (2016) 23–34.
[41] A. Sinha, R. Gupta, J.A. Nairn, Thermal degradation of bending properties of structural wood and wood-based composites, Holzforschung 65 (2011) 221–229.
[42] H. Yoshihara, T. Furushima, Shear strengths of wood measured by various short beam shear test methods, Wood Sci. Technol. 37 (2003) 189–197.
[43] U. Ayata, L. Gurleyen, B. Esteves, T. Gurleyen, N. Cakiciere, Effect of heat treatment (ThermoWood) on some surface properties of parquet beech (Fagus orientalis Lipsky.) with different layers of UV system applied, BioResources 12 (2017) 3876–3889.
[44] D. Kačíková, F. Kačík, I. Čabalová, J. Ďurkovič, Effects of thermal treatment on chemical, mechanical and colour traits in Norway spruce wood, Bioresour. Technol. 144 (2013) 669–674.
[45] Y. Ding, O.A. Ezekoye, S. Lu, C. Wang, Thermal degradation of beech wood with thermogravimetry/Fourier transform infrared analysis, Energy Convers. Manag. 120 (2016) 370–377.
[46] Bauchau O.A., Craig J.I. Euler-Bernoulli beam theory, 2009, p. 173–221.